Received: 6 October 2022 | Accepted: 1 November 2022

DOI: 10.1002/pamm.202200110

A Machine Learning Enabled Image-data-driven End-to-end Mechanical Field Predictor For Dual-Phase Steel

Binbin Lin[1,*], **Setareh Medghalchi**[2], **Sandra Korte-Kerzel**[2], and **Bai-Xiang Xu**[1]

[1] Mechanics of Functional Materials Division, Institute of Materials Science, Technische Universität Darmstadt, Darmstadt, Germany

[2] Institute for Physical Metallurgy and Materials Physics, RWTH Aachen University, Aachen, Germany

This contribution presents convolutional neural nets (CNN) based surrogate models for prediction of von Mises stress and equivalent plastic strain fields of commonly used Dual-Phase (DP) steels in automotive applications. The models predict field quantities in an end-to-end manner, driven by segmented phase images from real experimental scanning electron micrographs as inputs and FEM calculations as outputs. Hereby, we train CNN models with the U-net neural network structure based on around 900 elastoplastic FEM simulations of various DP steel microstructure samples under tensile test. The trained CNN models are validated and tested on 250 and 50 samples, respectively. Thereby CNN models are employed sequentially for different tasks , from the real micrographs to segmented phase maps, then from segmented phase maps to stress, strain field predictions, in an end-to-end manner. The field predictor model results show good agreement with the test data and convincing performance on unseen microstructural dataset. This work demonstrates the large potential of a Machine Learning model to make accumulatively use of the physics-based simulation data of large number of boundary value problems with varying microstructure. It recaptures not only the physics, implied in each simulation training data obtained from the partial different governing equations of mechanics, but also the overarching correlation between the microstructure and the stress and strain field responses.

1 Introduction

Dual-Phase steels are a class of high-advanced steels with their microstructure constituents consisting of a soft ferrite and a hard martensite phase. Due to their extraordinary mechanical properties, they are widely used in automotive chassis. The general macroscopic mechanical properties are thus governed by their particular phase constituents and defects in the material system. However, their local mechanical responses, such as local stress, strain concentration and damage localization to external loading are challenging to predict due to their inherent complex morphological variations and accumulation of the phases at the same time [1]. Given the materials constitutive behavior of each constitute and interface, numerical simulations can be done in principle for each microstructure sample. However, due to the wide variation of microstructure features, large number of simulations are required, which implies high computational cost. Moreover, such individual simulation results have low transferability for unseen microstructural data and difficult to establish a straight-forward microstructure-property model and its relations. Recently, data-driven Machine Learning techniques, rooted in computer science, have been increasingly applied in other research fields, from bio-medicine to materials and mechanics science. In particular, deep learning models help to explore unseen microstructure and facilitate in building microstructure-property relations. There are surrogate ML models based on the user-defined or statistical microstructure feature descriptors [2,3]. A more straightforward surrogate model would be to use the microstructure image as input and the interested results as output, such as the stress/strain distribution throughout the microstructure. In this way, no simplifications have to be made on the real microstructure, which take consideration of voids, defects, details of different phases, spatial distributions in its best details. Prediction of field quantities further leads to simple calculation of averaged quantities, such as homogenized strain/stress, damage extent, including uncertainty measures. Extracted field properties can be used for modelling of macroscopic behaviour, multi-scale simulations. Given sufficient and representative datasets, such an end-to-end ML model promises high transferability of knowledge. For instance, the model can be used as a simple black-box-tool to help material scientists without computational domain expertise to understand and predict mechanical behaviours of the considered material system. The current contribution is structured follows: we firstly present the input and output data for the machine learning model, followed by brief introduction to the U-net model and its training details. We further discuss the training and testing results, and conclude with perspectives of future work.

2 Data Generation and Methodologies

The data generation workflow of the present work is divided in two parts, see Fig. 1. The first is concerned merely with the input experimental data, which is briefly introduced in the first subsection. Thereby details will be given on how to obtain the segmented micrographs from the paranomic image of dual phase steel sample. Based on the segmented phase images, we

* Corresponding author:b.lin@mfm.tu-darmstadt.de, xu@mfm.tu-darmstadt.de

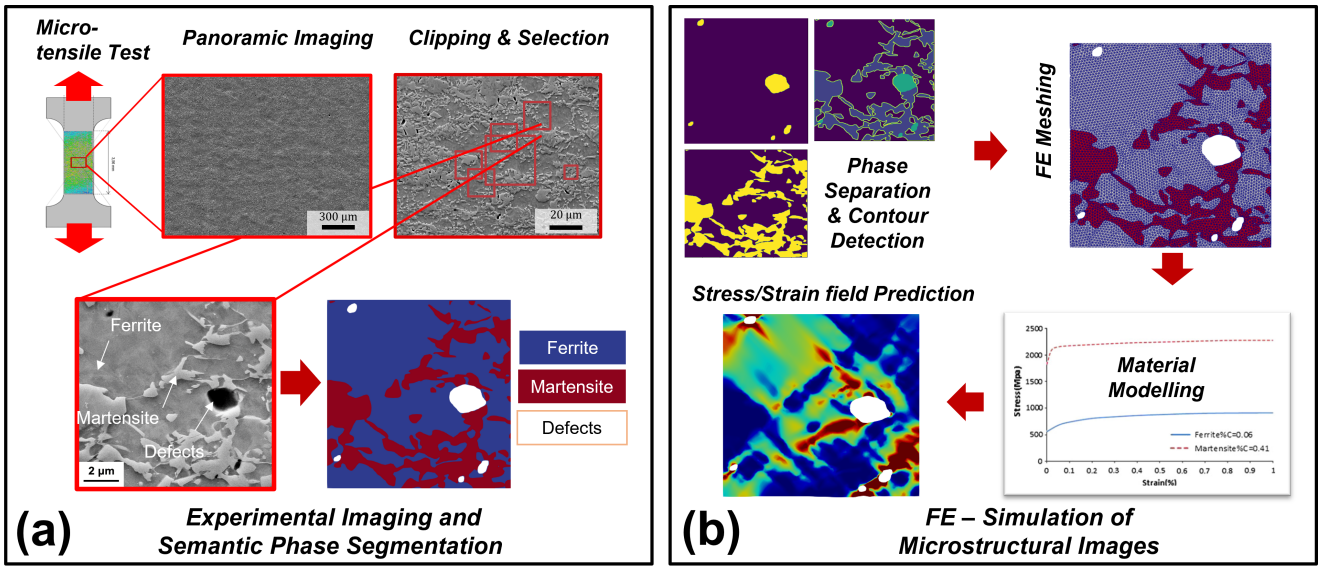

Fig. 1: Overall workflow of the data production process. Microstructural SEM-micrographs are obtained from micro-tensile test of Dual-Phase steel sample after panoramic imaging and clipping. The micrographas are then segmented semantically using machine learning based segmentation techniques. The segmented phase maps serve as input images for the U-net model and are contour-meshed for elastoplastic FE-simulations under tensile loading to obtain the local von Mises stress and equivalent plastic strain field, that serve as output image data for the predictive ML-model.

introduce in the second subsection the elastoplastic finite element simulations, results of which serve as the output of the ML model.

2.1 Input data: segmented microstructure phase maps

In the present study, the commercial DP800 Dual-Phase steel (ThyssenKrupp Steel Europe AG) has been investigated as a model system. As its marketing label addresses, this type of DP steel has at least 800 MPa tensile strength. The testing sample was cut out of 1.5 mm thick sheet metal to dog bone shape to be elongated uni-axially in the rolling direction. The sample was then cut to its necking area with an electron discharge machine (EDM). High resolution panoramic scanning electron microscope (SEM) images were collected from metallographically prepared areas with a size of 900 μm * 900 μm using secondary electrons of field emission scanning electron microscopes (LEO 1530; Carl Zeiss Microscopy GmbH, Jena, Germany) and TESCAN CLARA. The spatial resolution of the obtained images was 32.5 nm/pixel. The high resolution electron microscopic images of the microstructure were segmented using deep learning based convolutional neural networks [4] developed with Tensorflow 2.0.0. For this purpose, the panoramic images were cropped to smaller window sizes of 512 * 512 pixels. Subsequently, they were labelled manually using Image Labeler application of Matlab 2019 on randomly selected images. Here three known phases in the microstructure, ferrite, martensite and the defect phases were segmented. Since the manual labeling of the images was labour intensive, image augmentation algorithms were applied on the training data to boost the number of the images and increase the network accuracy. The network was trained at RWTH computer cluster with a GPU card of Nvidia V100. With the resultant network, all of the microstructural image were segmented and accordingly stitched. For training of stress/strain field predictors based on the segmented phase maps, we further randomly selected microstructure images with a windows size of 256 * 256. The size of microstructure samples should hold a good trade-off between the computation cost and the representativeness. Based on our preliminary investigation, we decided for this input size due to the number of martensite phases and their morphologies contained in this size of image. With larger image size, the computation cost to resolve the corresponding details increases unproportionally for both meshing and FE calculations.

2.2 Output data: FE-simulated field quantities

To carry out the FE-simulation, the segmented microstructural phase images were firstly meshed using a customized workflow based on the open-source meshing tool Gmsh. Here, we firstly separated the defects (white phase) and the martensite phases (red phase), which were considered as foreground objects by their pixel values. The ferrite phase (blue phase) was considered as the background color. Afterwards, contour detection on the foreground objects was performed, achieved by the *findContours* method with the OpenCV library in Python. These contour points were then transferred into Gmsh number formats and line loops were created for those contour objects. Further, a large ferrite contour was added to the contours which serve as background mesh for the material domain. Lastly, material assignment for different phases were performed, where mesh generation was skipped only for contours of defect phases to create "holes" in the simulation mesh domain. This procedure

has been then automated towards processing large database of microstructural images. After setting up the image-based mesh, FE-simulations at small strain with uni-axial tensile boundary conditions were performed using the open-source FE code MOOSE. Extension of the model to account finite deformation theory will be considered in our future work. The governing equations for a classical rate-independent plasticity models are briefly summarized, following [5]:

$$\mathrm{Div}\,\boldsymbol{\sigma} = 0 \quad \text{in} \quad \Omega, \qquad \mathbf{u} = \mathbf{u}_0 \quad \text{on} \quad \Gamma_u, \qquad \mathbf{t} = \mathbf{t}_0 \quad \text{on} \quad \Gamma_t, \tag{1}$$

where $\boldsymbol{\sigma}$ is the stress tensor and Ω is the image domain. The boundary conditions, either as displacement $\mathbf{u}$ or traction $\mathbf{t}$ boundary conditions, can be applied. The total strain tensor $\boldsymbol{\varepsilon}$ is defined as the symmetric part of the gradient of displacements within the small strain theory and classically decomposed by the split into the elastic and the plastic part $\boldsymbol{\varepsilon}_e$ and $\boldsymbol{\varepsilon}_p$:

$$\boldsymbol{\varepsilon} = \frac{1}{2}[\,\nabla\boldsymbol{u} + \nabla\boldsymbol{u}^T\,] \qquad \boldsymbol{\varepsilon} = \boldsymbol{\varepsilon}_e + \boldsymbol{\varepsilon}_p, \qquad \boldsymbol{\sigma} = \boldsymbol{C} : [\boldsymbol{\varepsilon} - \boldsymbol{\varepsilon}_p], \tag{2}$$

with the corresponding constitutive equation and $\boldsymbol{C}$ the forth-order elasticity tensor. We further assumed isotropic hardening conditions. When the material loaded beyond its yielding point, which is driven by the J_2-plasticity, governed by the second invariant of the deviatoric stress tensor $J_2 = \frac{1}{2}\boldsymbol{s} : \boldsymbol{s}$, with $\boldsymbol{s} = \boldsymbol{\sigma} - \frac{1}{3}\mathrm{tr}(\boldsymbol{\sigma})I$. The von Mises stress can be defined in the same regard as $\sigma_{v,M} = \sqrt{3J_2}$. The plastic flow rule, yield function and evolution of the hardening parameter are given as following:

$$\dot{\boldsymbol{\varepsilon}}_p = \gamma\frac{\partial f}{\partial \boldsymbol{\sigma}}, \qquad f = \|\boldsymbol{s}\| - \sqrt{\frac{2}{3}}K(\alpha), \qquad \dot{\alpha} = \sqrt{\frac{2}{3}}\gamma, \tag{3}$$

with $\gamma = \|\dot{\boldsymbol{\varepsilon}}_p\|$ and $\alpha = \int_0^t \dot{\alpha}\,\mathrm{d}t$ normally also denoted as the equivalent plastic strain (PEEQ) that defines isotropic hardening of the von Mises yield surface. Further, the loading-unloading is fulfilled by the Kuhn-Tucker conditions: $\gamma \geq 0, f \leq 0, \text{and } \gamma\ f = 0$. The hardening function K follows a linear hardening model for the martensite phase, and a power law hardening model for the ferrite phase:

$$K(\alpha) = \sigma_F + \bar{K}_F\alpha^n, \qquad \sigma = \sigma_M + \bar{K}_M\alpha. \tag{4}$$

Here, σ_F and σ_M denote the yield strengths and $\bar{K}_F$ and $\bar{K}_M$ the hardening coefficients for the ferrite and martensite phases, respectively. n denotes the hardening exponent for the ferrite phase. Due to the lack of material data of individual phases, we adapted the material parameters from [6] for an exemplary DP980 steel, with σ_F = 425 MPa, $\bar{K}_F$ = 940 MPa, n = 0.2 for the ferrite phase, σ_M = 1180 MPa and $\bar{K}_M$ = 1740 MPa for the martensite phase, respectively. We are aware that the exact material properties for our DP800 steel sample are different from these literature numbers. However, since the purpose of this contribution is to train an end-to-end CNN-model to predict the field quantities, we find still appropriate to use these material parameter set to perform FE-simulations generating output quantities for the model training as illustrative examples. Determination of the material parameters of the DP800 sample would be carried out in our future work. Computation of the trial stress and update of the plastic strain and stress increment were solved numerically with the radial return methods implemented in the MOOSE code [7].

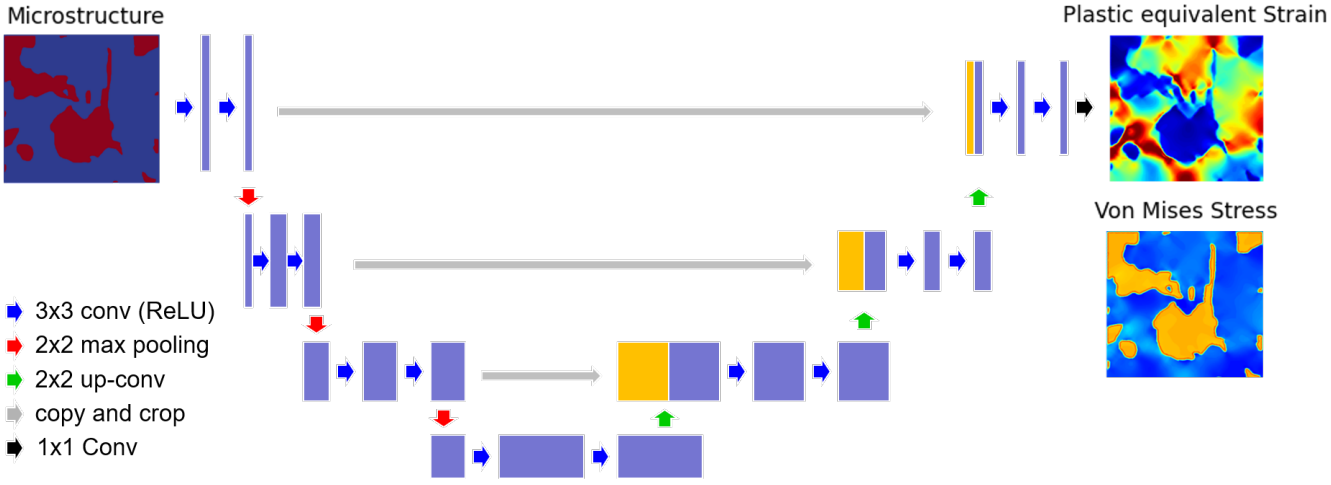

Fig. 2: A schematic sketch for the U-net structure: Input data is the segmented micrograph phase maps, while the output is either the plastic equivalent strain map or the von Mises stress map.

2.3 U-net model and training details

The U-net is a convolutional network architecture originally aimed for fast and precise segmentation of images. Our choice for U-net compared to other neural networks lies in its capability of extracting local features by convolution operations, as our microstructural morphology and stress/strain field have strong localized attribute without doubt. As for our end-to-end field mapping in this work, we utilized the U-net model in its unmodified form as proposed by [8]. The U-net model, see Fig. 2, consists of an contraction path, that learns to encode the features and follows the typical structure of a convolutional network, but with repeated application of convolution, ReLU activation, max pooling operations. The expansion path decodes the contracting path, by upsampling of the feature map with further convolutions and concatenation of previously cropped feature map from the encoding path. The reader is referred to [8] for more details. The U-net model is implemented in our code with the deep learning framework Pytorch, further improvement and modification of the network hyperparameters, as similarly performed in [9, 10] are sought in our further studies. For training of our field predictor, the input data of the model is the segmented microstructures with three phases, namely the ferrite , martensite and defect phases of only one channel with pixel intensity values ranging from 0 - 255. The output data of the model is either the PEEQ or the von Mises stress field image obtained from the elastoplastic FE-Simulations at last loading step. The field images were mapped to their undeformed configuration to assure the image size compatibility. In total, 1200 samples of segmented phase maps with their corresponding PEEQ and von Mises maps were generated and subsequently split into a 75/20/5% ratio, making 900 samples for training, 250 samples for validation and 50 samples for testing, respectively. Two models were separately trained for the strain and the stress field for 120 epochs with 4 images per batch. The learning rate was set to 5e-4. Adam optimizer with default settings by Pytorch during the training steps and the L1 loss was used. The model weights were saved every 10 epochs. Every epoch took approx. 5 to 6 minutes, and the training and validation finished in 6 – 8 hours running on 4 GPUs of type Nvidia A/V100. The loss curves for both models can be found in Fig. 3. As can be found in the learning curves, a trend of over-fitting can be found for both model training curves after approx. 30 epochs. Therefore, we decided to use the model weights at 30 epochs for testing the unseen dataset. Possible origin for this over-fitting event will be discussed in the later section.

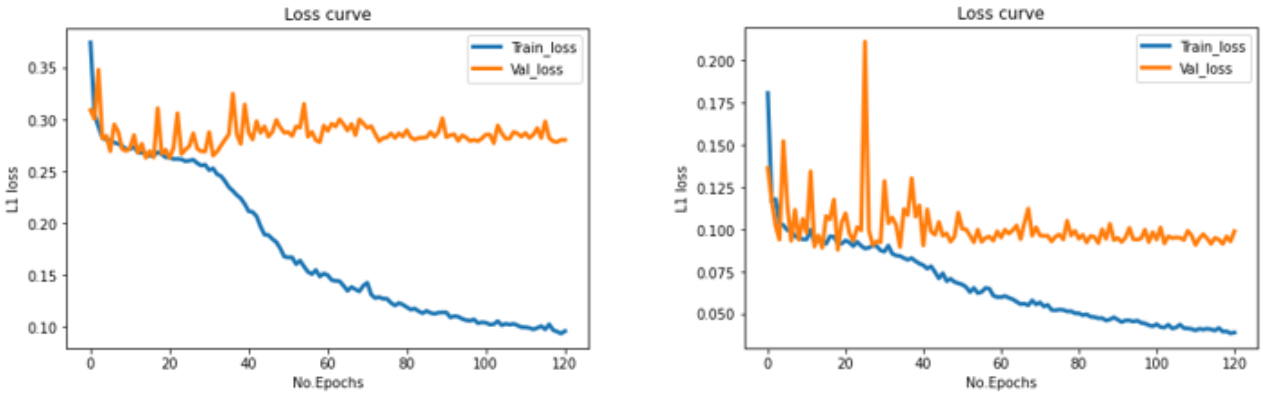

Fig. 3: Learning curves for the train and the validation losses; Left: Model training for the PEEQ map, Right: Model training von Mises stress map. A clear trend of over-fitting can be found for both model training curves after approx. 30 epochs.

3 Test data results and discussions

The model prediction results for exemplary unseen microstructure images are presented in Fig. 4, 5 for the PEEQ maps and von Mises stress maps, along with their ground truth data from FE-simulation and the pixel-wise error, respectively. Here, the first column shows exemplary microstructures, the second column shows the ground truth data, the third column shows the field prediction by the model and the pixel-wise error in the last column. The rows indicate the results for different microstructures. To measure the overall prediction performance, the percentage mean absolute error (PMAE) as in [11] is introduced:

$$\mathrm{PMAE} = \frac{\mathrm{MAE}}{\mathrm{Max}(Y) - \mathrm{Min}(Y)} \text{ x } 100\%, \qquad \mathrm{MAE} = \frac{1}{N}\sum |y^i_{gt} - y^i_{predict}| \tag{5}$$

with $\mathrm{Max}(Y)$, $\mathrm{Min}(Y)$ denote the maximum and minimum pixel value of the image Y, and $|y^i_{gt} - y^i_{predict}|$ the absolute error between the i^{th} ground truth pixel value and the model-predicted pixel value of the PEEQ or the von Mises stress field image. N is the number of pixels within one considered image. As can be found in 4, for the first two microstructure samples without any defect phase, the plastic strain regions are mostly located in the ferrite phase, due to its lower stiffness and earlier plastification, mainly around the sharp edges of the martensite phase. These plastic strain localization patterns are qualitatively well captured by the ML-prediction compared to the PEEQ ground truth FE data. However, the error column indicates still

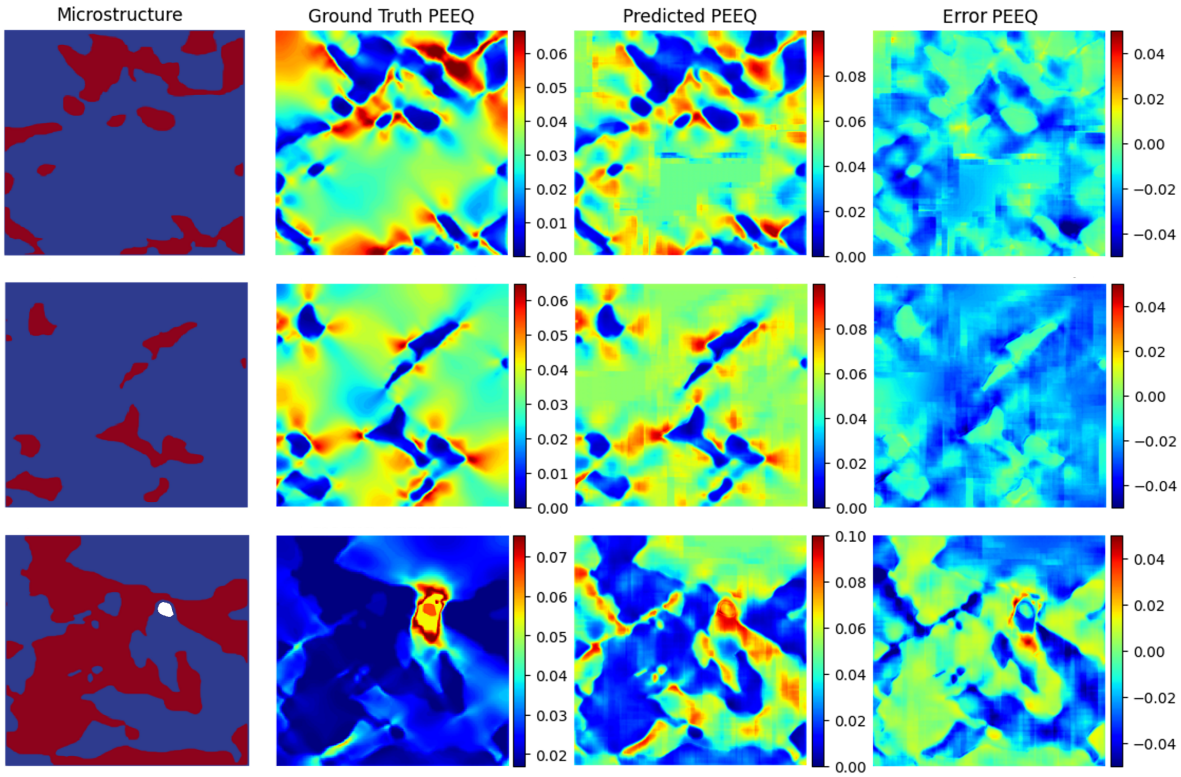

Fig. 4: PEEQ prediction results by the U-net model for exemplary microstructures. First column: Exemplary microstructures; Second column: Ground truth PEEQ field calculated by FE-simulation; Third column: Predicted field results by the U-net model; Forth column: The pixel-wise error between ground truth and the model prediction.

minor deviation in some sharp region around the martensite phase, and the pixelated nature of model prediction. As for the third exemplary microstructure involving a small defect inclusion, large deviation were observed for model prediction compared to the ground truth data. Apparently, the model missed the plastic strain concentrations around the defect inclusion and predicts a rather homogeneous strain distributions following the previous pattern, hence leading also to larger overall deviations. In total, the PMAE of the PEEQ field predictor scores around 14 ± 3.5 % for the whole test dataset of 50 microstructure samples. Similar results can be found for the von Mises stress prediction in Fig. 5. While the trained machine-learning model predicts acceptable results for other similar microstructure without defects, increasing deviations are existent and can be found for a microstructure containing a similar defect inclusion. Nevertheless, the stress predictor performs slightly better and captures the stress concentration in the vicinity of the defect compared to the strain predictor. Yet still larger deviation at the martensite boundaries can be found in the error map. The score for the von Mises stress predictor is $\mathrm{PMAE} = 11 \pm 4.2$ %. We assume that the lower prediction performance for microstructure with defect phases of both strain/stress predictors originates from the large data imbalance within the phase distributions among ferrite, martensite and defect pixels in the training dataset. The defect phase currently represent 0.2% of the total pixels from the whole paranomic image. By the uniform random sampling and cropping of the paranomic image data, the total defect phase pixels also correspond to this approximate fraction in our training dataset. To miltigate this issue, a different sampling technique and augmentation techniques to balance out the defect phase should be considered in the future work.

4 Conclusion and outlooks

In this work, we presented a end-to-end field predictor for strain and stress field predictions of Dual-Phase steel microstructures from real SEM images, based on the deep learning model U-net. This is enabled by training the model using segmented microstructure phase graphs as input data and the elastoplastic FE-simulation results as the output data. The results demonstrate promising potential in using the U-net model for accurate mechanical stress and strain field prediction, enabling a facile knowledge transfer from computational simulation to experimental material science domain, as well as accelerating the stress/strain analysis and further to robust, material design. Future works include the extension of the small deformation theory to finite deformation, and the consideration of material damage models to study the microstructure-damage pattern correlation at the modelling level. As for the machine learning model, hyperparamter tuning, modification of the training data and generation of a larger dataset to mitigate the data imbalance issues with respect to the defect phase will be carried out.

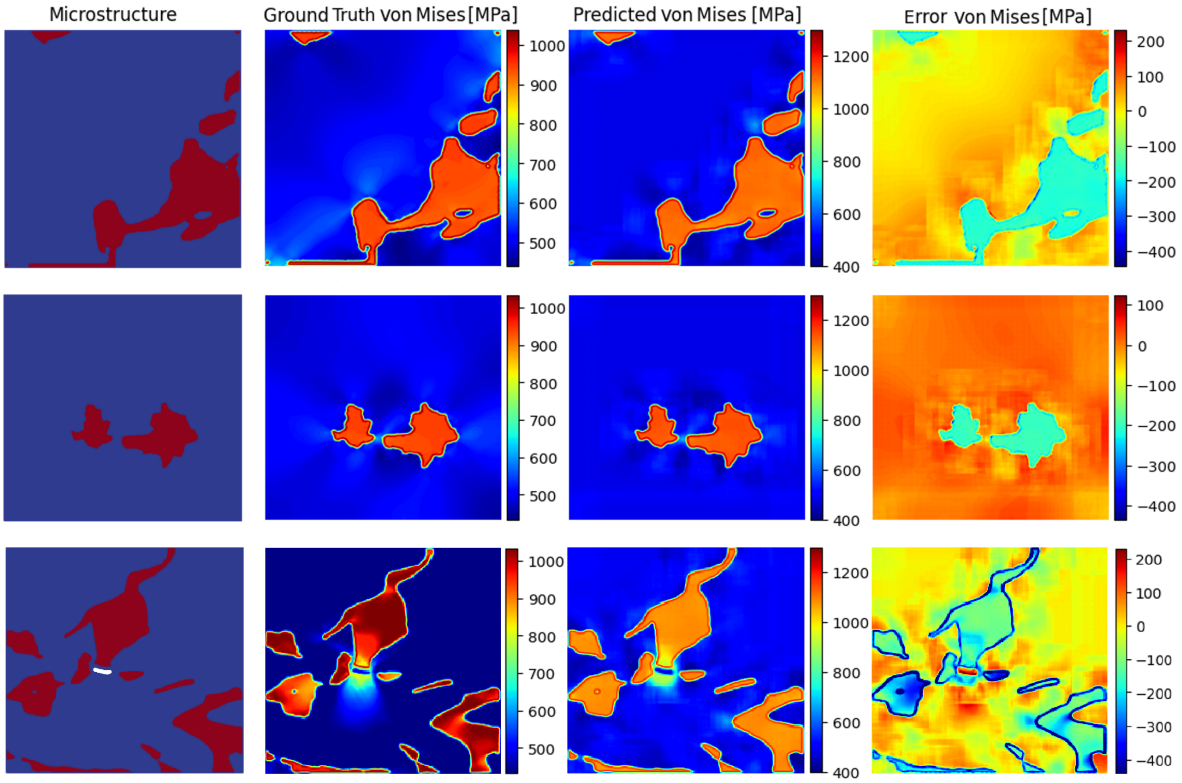

Fig. 5: Von Mises sterss prediction results by the U-net model for exemplary microstructures. First column: Exemplary microstructures; Second column: Ground truth stress field calculated by FE-simulation; Third column: Predicted field results by the U-net model; Forth column: The pixel-wise error between ground truth and the model prediction.

Acknowledgements The authors gratefully acknowledge the financial support and the computing time provided to them at the NHR Center NHR4CES at RWTH Aachen University (project number 0535) and TU Darmstadt (project number project1020, special0007). This is funded by the Federal Ministry of Education and Research, and the state governments participating on the basis of the resolutions of the GWK for national high performance computing at universities (www.nhr-verein.de/unsere-partner). Open access funding enabled and organized by Projekt DEAL.

References

[1] C. C. Tasan, M. Diehl, D. Yan, M. Bechtold, F. Roters, L. Schemmann, C. Zheng, N. Peranio, D. Ponge, M. Koyama et al., Annual Review of Materials Research **45**, 391–431 (2015).
[2] R. Ramprasad, R. Batra, G. Pilania, A. Mannodi-Kanakkithodi, and C. Kim, npj Computational Materials **3**(1), 1–13 (2017).
[3] B. Lin, Y. Bai, and B. X. Xu, Materials & Design **197**, 109193 (2021).
[4] S. Medghalchi, C. F. Kusche, E. Karimi, U. Kerzel, and S. Korte-Kerzel, JOM **72**(12), 4420–4430 (2020).
[5] J. C. Simo and T. J. Hughes, Computational inelasticity (Springer Science & Business Media, 2006).
[6] X. Sun, K. S. Choi, W. N. Liu, and M. A. Khaleel, International Journal of Plasticity **25**(10), 1888–1909 (2009).
[7] C. J. Permann, D. R. Gaston, D. Andrš, R. W. Carlsen, F. Kong, A. D. Lindsay, J. M. Miller, J. W. Peterson, A. E. Slaughter, R. H. Stogner et al., SoftwareX **11**, 100430 (2020).
[8] O. Ronneberger, P. Fischer, and T. Brox, U-net: Convolutional networks for biomedical image segmentation, in: International Conference on Medical image computing and computer-assisted intervention, (Springer, 2015), pp. 234–241.
[9] J. R. Mianroodi, N. H Siboni, and D. Raabe, Npj Computational Materials **7**(1), 1–10 (2021).
[10] M. S. Khorrami, J. R. Mianroodi, N. H. Siboni, P. Goyal, B. Svendsen, P. Benner, and D. Raabe, arXiv preprint arXiv:2208.13490 (2022).
[11] H. Jiang, Z. Nie, R. Yeo, A. B. Farimani, and L. B. Kara, Journal of Applied Mechanics **88**(5) (2021).

